PHYSICAL REVIEW B VOLUME 12, NUMBER 10 15 NOVEMBER 1975

Exact results for a three-dimensional alloy with site diagonal disorder: comparison with the coherent potential approximation

R. Alben*
Department of Engineering and Applied Science, Yale University, New Haven, Connecticut 06520

M. Blume†
Brookhaven National Laboratory, Upton, New York 11973
and Department of Physics, State University of New York, Stony Brook, New York 11794

H. Krakauer and L. Schwartz‡
Department of Physics, Brandeis University, Waltham, Massachusetts 02154
(Received 23 June 1975)

Densities of states and spectral functions are obtained for large (~8000 atoms) three-dimensional alloy models with cell localized disorder and are compared with the single-site coherent-potential approximation (CPA). We find that the CPA agrees remarkably well with the exact numerical results. In particular, the overall structure of the electronic spectrum and the transition from one- to two-band behavior are well described. There is, however, some substructure which is not reproduced by the single-site approximation.

There has been considerable interest over the last years in the electronic properties of substitutional disordered alloys and in the development of theoretical techniques for their description.[1] Of the various methods available, it is generally agreed that the most reliable is the coherent-potential approximation (CPA).[2,3] The CPA, in addition to being conceptually elegant, exhibits correct behavior in both the weak scattering and dilute limits and compares well with exact results on the limits of the allowed energy spectrum and the values of its leading moments.[4] Nevertheless, the CPA is a single-site approximation and is thus incapable of describing effects due to multisite correlations. In the case of one-dimensional models these effects have been shown to lead to serious discrepancies when comparisons are made to exact numerical calculations.[5] It is of interest to clarify the extent to which such discrepancies persist in three-dimensional systems, but accurate numerical solutions for large three-dimensional models have not been previously available.[6]

In this paper we present results for three-dimensional periodic models with about 8000 sites. By comparison, the three-dimensional models treated in Ref. 6 contain on the order of 1000 sites. The present models are simple cubic structures with a repeat distance of approximately 20 sites along the three Cartesian directions. We consider only site diagonal disorder, since this is the case in which the CPA is most easily implemented. The one-electron Hamiltonian may be written

$$H = v\sum_{i=j}{}' |i\rangle\langle j| + \sum_i |i\rangle \epsilon_i \langle i| \ , \qquad (1)$$

where the prime indicates that only nearest-neighbor pairs are included in the summation, v is the nearest-neighbor transfer integral, and ϵ_i is a site energy which takes the value $-\frac{1}{2}\delta$ or $\frac{1}{2}\delta$ depending on whether the site i is occupied by a B or an A atom. In the present calculations, a fraction c of the sites are specified at the outset to be of type A. We then solve the time-dependent Schrödinger equation numerically for a time interval determined by our desired energy resolution. The choice of initial conditions depends on whether we wish to calculate densities of states or spectral functions (see the Appendix). The resulting time behavior is then Fourier analyzed to give the final results. In each case we obtain exactly the spectrum of the finite model, broadened with a resolution function whose width is predetermined.[7] This method is extremely efficient since it does not require the use of large matrices as, for example, in the procedure of Bell and Dean[8] (see also Ref. 9).

In Figs. 1 and 2 the CPA is compared with numerical results for the density of states in a periodic model with 7980 sites (that is, $19\times20\times21$). The size of the model was chosen to provide a statistically significant number of different configurations (including the effects of rather long-range correlations) without consuming extravagant quantities of computer time and storage. The dimensions were purposely made asymmetrical to minimize degeneracies introduced by cubic symmetry. In each case, computations were carried out for four statistically independent distributions of impurities. We show separately the averages of pairs of runs and the grand average of all four

runs. Structure which is common to both pair averages is almost certainly characteristic of a typical alloy model of this size. Except for the oscillations in the majority (B) band for low c (see below) this common structure may be assumed to describe the spectrum of an infinite alloy sample.

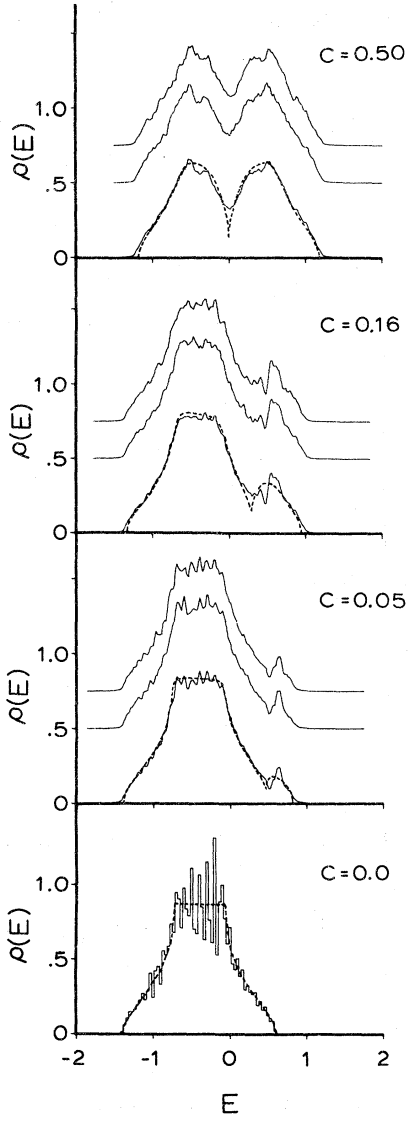

FIG. 1. Density of states for four concentrations c, of atoms of type A. Solid curves give the numerical results for 7980-site models; broken curves give corresponding CPA results. Case $c=0$ corresponds to a pure material for which the CPA result is exact. Finite-model result for the pure case is a simple histogram of the modes of the model. For $c \neq 0$, the density of states was obtained as described in the Appendix. Full width at half-maximum of the resolution function is 0.03 energy units, the same as the bar width of the histogram for the $c=0$ case. Upper two curves for each concentration are each averages of results for two statistically uncorrelated phases and distributions of impurities, and the lower curve is the average of the upper curves.

The results shown in Fig. 1 correspond to $\delta = 0.8$ and the impurity concentrations $c = 0.50$, 0.16, 0.05, and 0.0. The value $\delta = 0.8$ is of interest because the CPA results predict that in this case the alloy spectrum is on the verge of splitting into two distinct bands. The present machine computations indicate that this is indeed the case and show, further, that the CPA accounts quite well for the over-all band shape. On the other hand, the exact spectrum is seen to be spread over a slightly larger range of energies than that predicted by the CPA. This discrepancy is expected, since the states near the limits of the allowed spectrum are associated with large single component clusters and, as such, are beyond the scope of any single-site approximation. In addition we note that there is some substructure in the present result which does not appear in the CPA curves. (In connection with this final point we emphasize that the oscillations which develop in the majority band as $c \to 0$ are due to the nonuniform distribution of eigenvalues in the pure 7980-site crystal and are thus a finite size effect.)

In Fig. 2(a) we show the density of states for

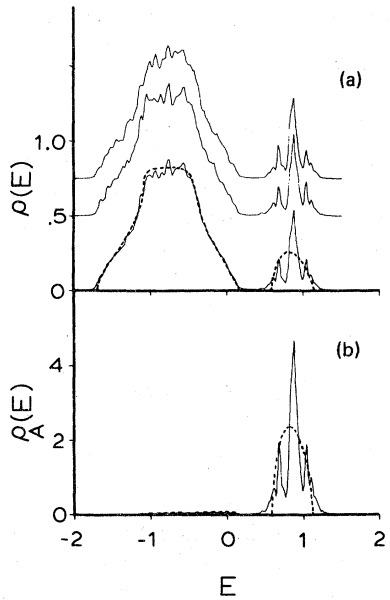

FIG. 2. (a) Density of states for $\delta = 1.5$ and $c = 0.1$. Solid curves are for 7980-site models; broken curves are CPA results. Lower curve is the average of the results, shown in the upper curves, for different impurity distributions and phases. (b) Minority component of the density of states for $\delta = 1.5$ and $c = 0.1$. Energy resolution is 0.03 energy units. Small magnitude of the minority component in the region of the majority subband is quite accurately given by the CPA.

$\delta = 1.5$ and $c = 0.1$. In this case the A and B subbands are well separated, and there is a three-peaked structure (with some substructure) evident in the minority band. Physically, the central peak in the minority band is due to isolated impurities, while the two satellite peaks arise from the bonding and antibonding levels of a nearest-neighbor impurity pair cluster.[10] This three-peaked behavior is also apparent in Fig. 2(b), where we show the minority component of the density of states. Although the single-site CPA cannot reproduce the detailed structure with the A subband, it does describe properly the over-all features of the spectrum.

We consider next the separate contributions to the alloy density of states associated with each vector $\vec{k}$ of the Brillouin zone. The contributions are given by the spectral function $A(\vec{k}, E)$:

$$\rho(E) = N^{-1} \sum_{\vec{k}} A(\vec{k}, E) \ , \tag{2}$$

where N is the total number of atoms in the model. In Fig. 3 machine calculations of $A(\vec{k}, E)$ are compared with their CPA counterparts. Results are shown for $\delta = 0.75$, $c = 0.10$, and four values of $\vec{k}$ corresponding to three points along the Λ line and one point along the $\sum$ line in the Brillouin zone. Within the CPA, $A(\vec{k}, E)$ depends on $\vec{k}$ only through the simple cubic energy-band function:

$$s(\vec{k}) = \tfrac{1}{3}(\cos k_x a + \cos k_y a + \cos k_z a) \ , \tag{3}$$

where a is the lattice constant. The curves in Fig. 3 correspond to $s(\vec{k}) = -1$, $s(\vec{k}) = 0$ (two k vectors), and $s(\vec{k}) = -1$. It is particularly interesting to compare the two $s(\vec{k}) = 0$ curves and note that despite the fact that the first seven of the moments

$$M_p(\vec{k}) = \int_{-\infty}^{\infty} A(\vec{k}, E) E^p dE \tag{4}$$

[i.e., $M_0(\vec{k}) - M_6(\vec{k})$] are the same,[4] and are given correctly by the CPA, there are significant differences between the two curves and between them and the CPA results.

The case $\delta = 0.75$, $c = 0.10$ is on the borderline between one- and two-band behavior, as may best be seen from the spectral function for $k = 0$. Here the weight is primarily at the upper limit of the spectrum, with just a small contribution at the edge of the majority subband. By contrast, in Fig. 4 we show a case corresponding to clear two-band behavior. Here $\delta = 1.5$, and the minority subband is split off. For $k = 0$ the principal peak is at the upper edge of the majority band. We note also that the minority subband is split into two peaks. These correspond, respectively, to isolated impurities and to the bonding states of pair clusters. {The antibonding states [cf. Fig. 2(b)] do not contribute at $k = 0$.} As in the case of the total density of states, there is again good qualitative agreement between the CPA and the numerical results.

In summary, the present calculations indicate

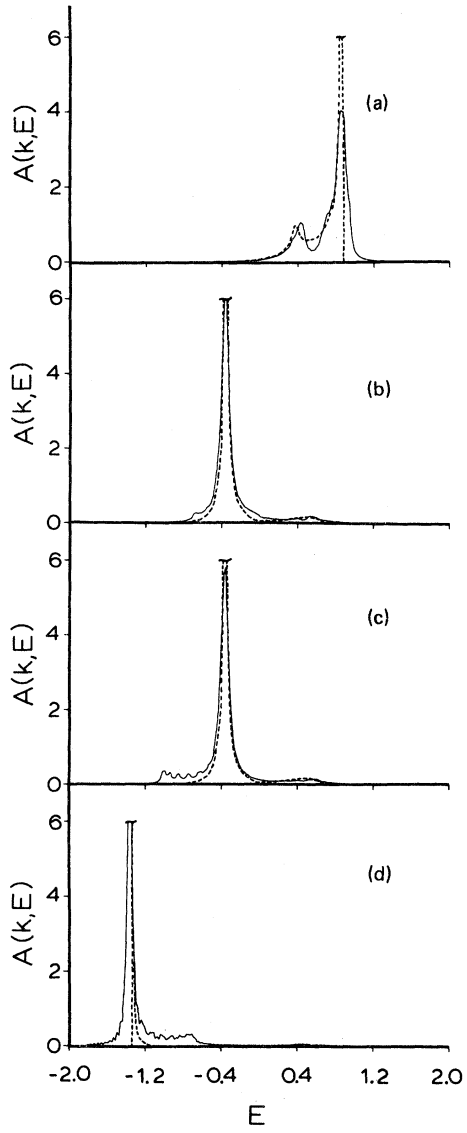

FIG. 3. Spectral function $A(k, E)$ for $\delta = 0.75$ and $c = 0.10$. Solid curves are for models; broken curves are CPA results. (a) $\vec{k} = (0, 0, 0)$, $s(\vec{k}) = 1$, model dimensions: $20 \times 20 \times 20$; (b) $\vec{k} = (\frac{1}{2}, \frac{1}{2}, \frac{1}{2})(\pi/a)$, $s(\vec{k}) = 0$, model dimensions: $20 \times 20 \times 20$; (c) $\vec{k} = (\frac{2}{3}, \frac{2}{3}, 0)(\pi/a)$, $s(\vec{k}) = 0$, model dimensions: $21 \times 21 \times 18$, and (d) $\vec{k} = (1, 1, 1)(\pi/a)$, $s(\vec{k}) = -1$, model dimensions: $20 \times 20 \times 20$. For cases (b) and (c), the results in the region of the peak agree to within the energy resolution of the numerical results. For case (d), the peak is considerably broader for the model spectrum than for the CPA for which the intensity rises very sharply at the CPA-computed band edge.

that the CPA does describe properly the essential features of the alloy's electronic spectrum. That the agreement between the machine calculations and the CPA results is much better in three- than in one-dimensional systems is not surprising, since the CPA is a mean-field theory and corrections to it are expected to scale as Z^{-1} (where Z is the lattice coordination number).[11]

APPENDIX: OUTLINE OF THE EQUATION-OF-MOTION PROCEDURE

We consider the N-site system defined by the Hamiltonian (1) and introduce the retarded Green's functions

$$G_{ij}(t) \equiv -i\langle 0|c_i(t)c_j^\dagger(0)|0\rangle \ , \quad t \geq 0 \ , \tag{A1}$$

where $c_j^\dagger(0)$ creates an electron at site j at time zero, $c_i(t)$ destroys an electron at site i at time t, and $\langle 0|$ is the state with all orbitals empty. We next write N Green's functions which refer to the amplitudes at each site associated with an initial excitation of wave vector $\vec{k}$:

$$\tilde{G}_{i\vec{k}}(t) = \frac{1}{N}\sum_j e^{i\vec{k}\cdot\vec{R}_j} G_{ij}(t) \quad (i = 1, N) \ , \tag{A2}$$

where $\vec{R}_j$ is the position vector of site j.

The $\tilde{G}_{i\vec{k}}$'s can be conveniently calculated from their equations of motion:

$$i\hbar\frac{\partial}{\partial t}\tilde{G}_{i\vec{k}}(t) = v\sum_j{}' \tilde{G}_{j\vec{k}}(t) + \epsilon_i \tilde{G}_{i\vec{k}}(t) \ , \tag{A3}$$

with initial conditions

$$\tilde{G}_{i\vec{k}}(0) = -i e^{i\vec{k}\cdot\vec{R}_i} \ , \tag{A4}$$

where the primed sum in (A3) is over nearest neighbors of i. Equation (A3) can be accurately replaced by the difference equations

$$\tilde{G}_{i\vec{k}}(t+\delta) = \tilde{G}_{i\vec{k}}(t-\delta) + \frac{2\delta}{i\hbar}\left(v\sum_j{}' \tilde{G}_{j\vec{k}}(t) + \epsilon_i \tilde{G}_{i\vec{k}}(t)\right), \tag{A5}$$

where δ is the time step for each iteration cycle.[12] We have found that $\delta \lesssim \frac{1}{20}$ of the shortest time period for the system gives an accuracy better than 1% in our final spectra. (The shortest time period is Planck's constant divided the maximum absolute value of the energy.)

The spectral function for wave vector $\vec{k}$ is written

$$A(k, E) = \lim_{\lambda \to 0^+} \frac{1}{\pi}\,\mathrm{Im}\left(\frac{1}{\hbar}\int_0^\infty \sum_i e^{-i\vec{k}\cdot\vec{R}_i}\tilde{G}_{i\vec{k}}(t)e^{iEt/\hbar - \lambda t}dt\right) . \tag{A6}$$

In our procedure, we replace (A6) by a sum of terms corresponding to an integration time T. Typically, $T \approx 250\delta$. The principal effect of this approximation is to produce a broadening of the spectrum. (The value of λ is chosen to effectively suppress termination oscillations without adding unnecessarily to the broadening.) For the results reported here the broadening corresponds to a resolution full width at half-maximum of 0.03 energy units. The calculation of $A(\vec{k}, E)$ for one wave vector as a function of energy at this resolution takes 20 sec on a CDC 7600 computer for 8000-site models. Approximately 5×8000 storage locations are required.

The density of states was obtained from a spectral function for "incoherent scattering." That is, the phase $\vec{k}\cdot\vec{R}_i$ in Eqs. (A2), (A4), and (A6) were

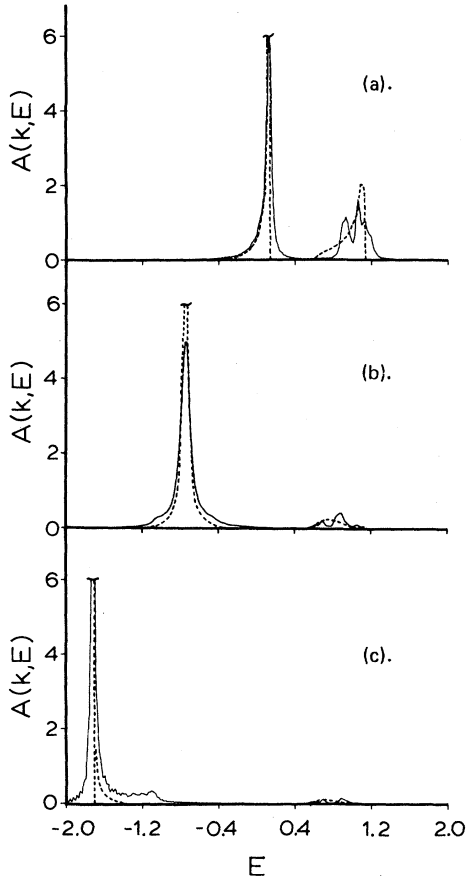

FIG. 4. Spectral function $A(k, E)$ for $\delta = 1.5$ and $c = 0.10$. Solid curves are for $20\times 20\times 20$ models; broken curves are CPA results. Curves are cut off at six units for ease of presentation. (a) $\vec{k} = (0, 0, 0)$, $s(\vec{k}) = 1$; (b) $\vec{k} = (\frac{1}{2}, \frac{1}{2}, \frac{1}{2})(\pi/a)$, $s(\vec{k}) = 0$; and (c) $\vec{k} = (1,1,1)$ (π/a), $s(\vec{k}) = -1$. For case (b), the results in the region of the peak agree to within the energy resolution of the numerical results. For case (c), the peak is considerably broader for the model spectrum than for the CPA.

replaced by random phases ϕ_i. With this replacement the spectral function $\rho'(\{\phi\}, E)$ for a particular set of phases $\{\phi\}$ is

$$\rho'(\{\phi\}, E) = \lim_{\lambda \to 0^+} \frac{1}{\pi} \operatorname{Im}\left(\frac{1}{\hbar}\int_0^\infty \frac{1}{N}\sum_{ij} e^{-i(\phi_i - \phi_j)} \times G_{ij}\, e^{iEt/\hbar - \lambda t}\, dt\right). \tag{A7}$$

We next average ρ' for a number M of independent sets $\{\phi\}$. This amounts to averaging the phase factors $e^{i(\phi_i - \phi_j)}$ in (A7), since no other terms depend on $\{\phi\}$. For $i \neq j$, the averaged phase factor is a random variable with a mean value of *zero* and a standard deviation which behaves as $M^{-1/2}$ for large M. From this it is straightforward to prove that when M is large, the terms in the double sum in (A7) referring to different sites will average to zero. This leaves a single sum of the site diagonal Green's functions which gives the true density of states. Averaging over a finite number of $\{\phi\}$'s leads to an approximate density of states in which the weighting of each mode varies about unity with a standard deviation which is about $M^{-1/2}$. (The deviation is somewhat less for highly localized states.) In practice, the statistical uncertainty associated with taking a single ρ' is quite comparable to that associated with different randomly occurring distributions of impurities. As may be seen from Figs. 1 and 2, the total uncertainty due to both of the above variations is quite small, and acceptable results may be obtained from averaging just a few calculations with independently chosen impurity distributions and phases.

---

*Supported in part by the National Science Foundation under Grant No. DMR-73-02627.

†Work at Brookhaven supported by the Energy Research and Development Administration.

‡Supported in part by the National Science Foundation under Grant No. DMR 72-03209.

[1]See, for example, R. J. Elliott, J. A. Krumhansel, and P. L. Leath, Rev. Mod. Phys. 46, 465 (1974).

[2]D. W. Taylor, Phys. Rev. 156, 1017 (1967).

[3]P. Soven, Phys. Rev. 178, 1136 (1969).

[4]B. Velický, S. Kirkpatrick, and H. Ehrenreich, Phys. Rev. 175, 747 (1968).

[5]P. Dean and M. D. Bacon, Proc. R. Soc. Lond. A 263, 64 (1965); W. H. Butler, Phys. Rev. B 8, 4499 (1973).

[6]D. N. Payton and W. M. Visscher, Phys. Rev. 154, 802 (1967).

[7]R. Alben, L. von Heimendahl, and M. F. Thorpe (unpublished); R. Alben and M. F. Thorpe, J. Phys. C 8, L275 (1975).

[8]R. J. Bell, Rep. Prog. Phys. 35, 1315 (1972); P. Dean, Rev. Mod. Phys. 44, 127 (1972).

[9]W. K. Holcomb and A. B. Harris, AIP Conf. Proc. 20, 102 (1975); S. Kirkpatrick and A. B. Harris, Phys. Rev. B (to be published).

[10]L. Schwartz and H. Ehrenreich, Phys. Rev. B 6, 2923 (1972).

[11]L. Schwartz and E. Siggia, Phys. Rev. B 5, 383 (1972).

[12]The considerations in solving these equations are quite similar to those encountered in molecular-dynamics calculations. See, for example, A. Rahman, Phys. Rev. 36, A405 (1964).